Renewable and Sustainable Energy Reviews 16 (2012) 1754–1761

Contents lists available at SciVerse ScienceDirect

Renewable and Sustainable Energy Reviews

journal homepage: www.elsevier.com/locate/rser

Control techniques for reduction of the total harmonic distortion in voltage applied to a single-phase inverter with nonlinear loads: Review

R. Ortega [a,b,*], E. Figueres [b], G. Garcerá [b], C.L. Trujillo [b,c], D. Velasco [b]

[a] Escuela Superior de Cómputo – Instituto Politécnico Nacional, Av. Juan de Dios Bátiz S/N, D.F., 07738 México, Mexico
[b] Grupo de Sistemas Electrónicos Industriales del Departamento de Ingeniería Electrónica, Universidad Politécnica de Valencia, Camino de Vera S/N, C.P. 46022, Valencia, Spain
[c] Departamento de Ingeniería Electrónica, Universidad Distrital Francisco José de Caldas, Carrera 7 N◦ 40-53 Piso 5, Bogotá, Colombia

ARTICLE INFO

Article history:
Received 5 April 2011
Received in revised form
14 November 2011
Accepted 25 November 2011
Available online 18 January 2012

Keywords:
Two-degree of freedom controller
Repetitive controller
Resonant controller
Inverter

ABSTRACT

This paper presents the design, analysis and implementation of four control techniques (proportional-integral, two-degree of freedom, repetitive and resonant) with the aim of reducing the total harmonic distortion in voltage (THD_v). When the inverter is working as a voltage source theses techniques are useful in island mode operation. The purpose is to keep the output voltage waveform, frequency and amplitude according to the standard IEEE 519, when nonlinear loads are fed. A comparative analysis derived from inverter simulations with nonlinear loads is realized in order to validate those control techniques.

Contents

1. Introduction

Today, most countries in the world used centralized generation, from thermoelectric, hydroelectric or nuclear power plants. These power plants are strategically located based on factors such as economic, safety, logistical or environmental. Many areas located in remote places do not receive adequate electricity service and transmission costs are expensive. Given those problems, the distributed generation (DG) [1] is an available solution since it reduces transportation costs because generation and consumption are close.

Under this new electricity generation scheme, it is feasible to implement interfaces with the ability of operating both in grid connected mode by injecting energy from renewable sources to the grid, and in islanding mode feeding local loads without grid connection. Those interfaces are known as microgrids [2]. Usually, microgrids are composed by low and medium voltage systems fed

* Corresponding author at: Escuela Superior de Cómputo – Instituto Politécnico Nacional, Av. Juan de Dios Bátiz S/N, D.F., 07738 México, Mexico.
E-mail addresses: rortegag@ipn.mx (R. Ortega), efiguere@eln.upv.es (E. Figueres), ggarcera@eln.upv.es (G. Garcerá), cltrujillo@udistrital.edu.co (C.L. Trujillo), davede@posgrado.upv.es (D. Velasco).

1364-0321/$ – see front matter
doi:10.1016/j.rser.2011.11.027

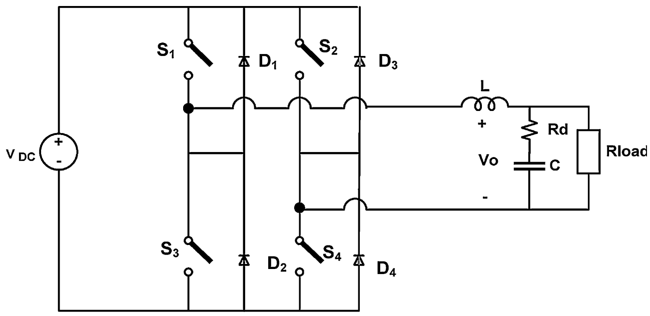


Fig. 1. Circuital scheme of the inverter.

Table 1
Parameters of the inverter under study.

Parameter	Values
Nominal active power (P)	3 kW
DC Link voltage (V_{DC})	400 V
Inverter output voltage (V_O)	230 V_{RMS}
Inverter output frequency (f_g)	50 Hz
Inverter inductance (L)	5.46 mH
Inverter output capacitor (C)	4.7 μF
Damping resistance (R_d)	5 Ω
Inverter switching frequency (f_{si})	16 kHz
Load resistance (R_{LOAD})	17.16 Ω

from distributed generation sources such as microturbines, fuel cells or photovoltaic systems together with energy storage devices and loads [3].

A microgrid is composed primarily by electronic equipment called inverters. The inverters working in a microgrid have the ability to operate both in island mode and in grid connected mode. It is important that the inverter imposes an appropriate voltage waveform operating in island mode. The voltage must comply with amplitude and frequency conditions, regardless of the type of load is connected [4]. Additionally, an adequate THD_V (less than 5% according to IEEE 519-1992) should be ensured [5,6]. This paper describes and analyzes four types of controllers to reduce THD_V. These controllers are: proportional-integral controller [7], two-degree of freedom controller [8], resonant controller [9] and repetitive controller [10].

2. Description of the implemented single-phase inverter

Fig. 1 shows the scheme of the H-bridge bipolar PWM inverter implemented. Table 1 summarizes the nominal values of the inverter.

For the design of the controllers it is necessary to identify the transfer functions of the variables to control. The transfer functions are extracted using the technique of switch modeling PWM [11]. The mathematical models that allow obtaining such transfer functions are presented in the next section.

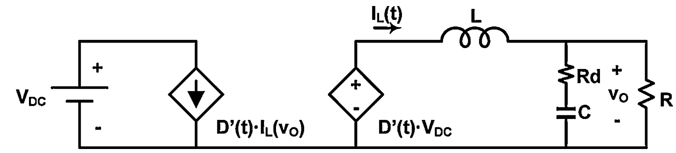


Fig. 2. Equivalent averaged model of the inverter around the operation point.

2.1. Small signal model of the inverter under study

To perform a linear feedback control from a circuit that is nonlinear as a switched converter, the power stage must be linearized. The switched converter has a small signal linear model for small perturbations around an operating point. From this model linear controllers can be designed to close control loops with different characteristics [12].

Fig. 2 shows the equivalent model of the inverter around the operation point. The inverter load is resistive. In Fig. 2 $D(t)$ is the duty cycle in the operation point and $D'(t) = 2{\cdot}D(t) - 1$.

Eq. (1) shows the expressions of the inductor current, $I_L(t)$, and the duty cycle, $D(t)$, at the operation point.

$$\begin{aligned} I_L(t) &= \frac{\sqrt{2}\cdot V_{O_RMS}}{R}\cdot\cos(\omega t) + \frac{\sqrt{2}\cdot V_{O_RMS}}{|Z_C|}\cdot\cos(\omega t - \varphi_C) \\ D(t) &= \frac{1}{2} + \frac{V_{O_RMS}}{\sqrt{2}V_{DC}}\cdot\left(-\frac{\omega\cdot L}{R}\cdot sin(\omega t) - \frac{\omega\cdot L}{|Z_C|}\cdot\sin(\omega t-\varphi_C) + \cos(\omega t)\right) \end{aligned} \tag{1}$$

where $|Z_C| = \sqrt{(R_d)^2 + (1/\omega\cdot C)^2}$ and $\varphi_C = \arctan(-1/\omega{\cdot}C{\cdot}R_d)$.

Based on small perturbations around the operation point, the small signal model is established (Fig. 3) [13].

In Fig. 3, $\hat{v}_{DC}$, $\hat{i}_L$, $\hat{d}$, y, $\hat{v}_O$ are terms of small signal.

From the model in Fig. 3, the following transfer functions are obtained, duty cycle to inductor current, $G_{I_L d(s)}$, and inductor current to output voltage, $G_{V_O I_L(s)}$, in order to apply the design control scheme.

2.2. Description of the control scheme used in the inverter

The inductor current and output voltage, are controlled for the inverter, for which is implemented an average current control (ACC) [14]. This scheme is shown in Fig. 4. where $G_V(s)$ represents the voltage control loop controller; $G_s(s)$ represents the current control loop controller; $RD(s)$ is the transfer function of a digital delay of one switching period (T_s) defined as:

$$RD(s) = \frac{1-((s\cdot T_s)/2)+((s\cdot T_s)^2/12)}{1+((s\cdot T_s)/2)+((s\cdot T_s)^2/12)} \tag{2}$$

F_m is the gain of the bipolar PWM modulator, given by (3):

$$F_m = \frac{1}{V_{pp_Triangular}} = 1 \tag{3}$$

R_i is the gain of the current sensor ($R_i = 0.2$) and β is the gain of the voltage sensor ($\beta = 0.006$).

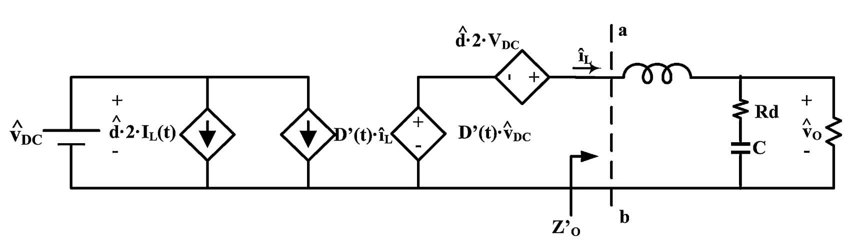


Fig. 3. Inverter small-signal model.

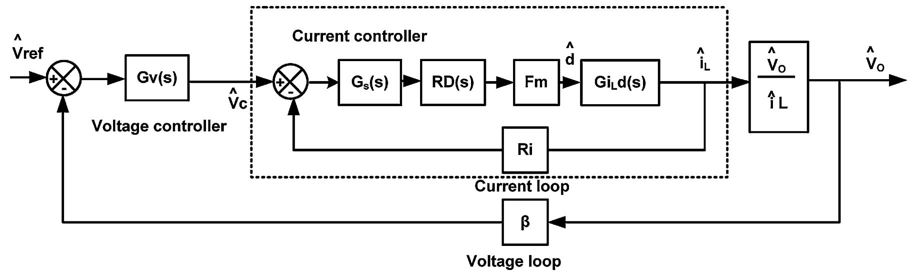


Fig. 4. Scheme of the average current control (ACC) for the inverter.

The transfer function of interest for the design of the current loop is that from the duty cycle to the output current, expressed by (4).

$$G_{i_L-d}(s) = \left.\frac{\hat{i}_L}{\hat{d}}\right|_{\hat{v}_{DC}=0} = \frac{2 \cdot V_{DC}}{Z_a + s \cdot L} \tag{4}$$

where Z_a is the load impedance in parallel with the output capacitor (5), and V_{DC} is the input voltage to the inverter.

$$Z_a = \left(R_d + \frac{1}{s \cdot C}\right) \bigg\| R = \frac{(s \cdot C \cdot R_d + 1) \cdot R}{s \cdot C(R_d + 1) + 1} \tag{5}$$

Fig. 5 shows the Bode plots of $G_{I_L d(s)}$.

The control scheme presented in Fig. 4 has the advantage of having a flatter response of the inductor current transfer function. Furthermore the controller exhibits less distortion than the current-injected control (CIC) [15] to generate alternating current.

The current mode control operates as follows: the voltage reference on the output voltage controller is supplied by an external reference that can be fixed or variable depending on its application.

The control of the inverter output voltage is performed through the controllers that will be set out in Section 4. It requires the current reference to the output current controller implemented through a resonant controller (or harmonic controller) and it will be set out in Section 3.

3. Current controller design

For the current loop a P + resonant controller [15] with the following transfer function has been chosen:

$$G_S(s) = K_p + \frac{K_h \cdot B_h \cdot s}{s^2 + B_h \cdot s + \omega_h^2} \tag{6}$$

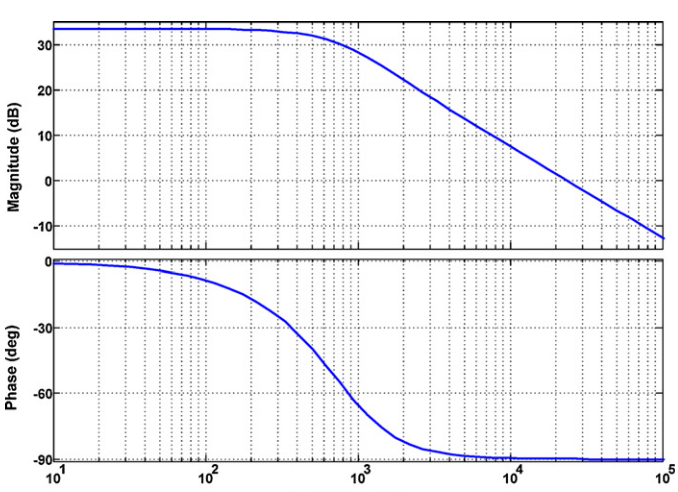


Fig. 5. Bode plots of $G_{I_L d(s)}$.

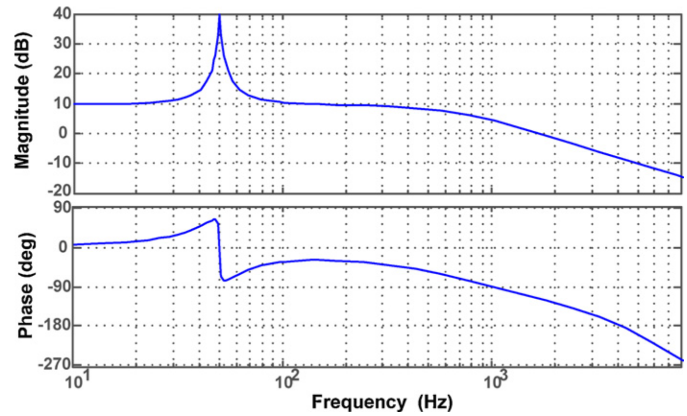


Fig. 6. Bode plots of current loop.

The proportional gain K_p can be determined by (7), where $\omega_{Ci_desired}$ is the desired crossover angular frequency of the current loop. In this case it is chosen: $\omega_{Ci_desired} = 2 \cdot \pi \cdot 1800$ rad/s.

$$K_p = \frac{L \cdot \omega_{Ci_desired}}{R_i \cdot F_M \cdot 2 \cdot V_{DC}} = 3.2 \tag{7}$$

For this application the following parameters have been chosen: $k_1 = 100$, $B_1 = 2 \cdot \pi$ rad, $\omega_1 = 2 \cdot \pi \cdot 50$ rad/s. The implementation of this controller produces a current loop with the following stability characteristics: $f_{Ci} = 1.92$ kHz (gain crossover frequency), PM = 62.1° (phase margin), GM = 8.2 dB (gain margin).

Fig. 6 shows the Bode plots of the current loop depicted in Fig. 4. It is defined as $T_i(s) = G_{i_L-d} \cdot F_m \cdot R_i \cdot G_s(s)$.

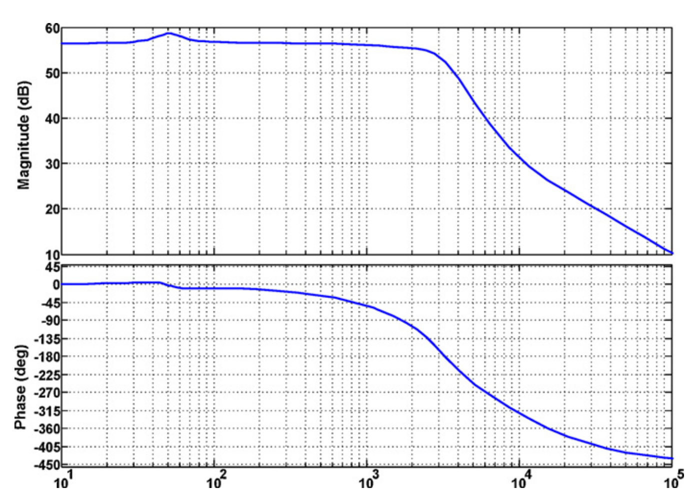


Fig. 7. Bode plots of $G_{v_O-v_C(s)}$.

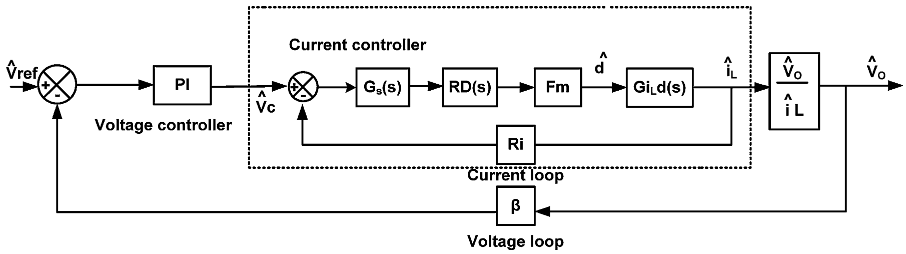


Fig. 8. ACC with PI controller.

4. Voltage controller design

The voltage controller regulates the inverter output voltage $\hat{v}_O$ and it sets the reference to the current controller. The control was implemented trough an average current control (ACC). It was developed with several controllers: Proportional integral controller (PI), two-degree of freedom controller (2DOF), resonant controller and repetitive controller.

These controllers aim to get a good reference tracking and to reduce the output voltage harmonic distortion when the inverter feeds linear and nonlinear loads. The controllers are described below.

For the design of the voltage controllers it is necessary to use the transfer function $G_{v_O-v_C}(s)$, which is determined as follows:

$$G_{v_O-v_C}(s) = \frac{\hat{v}_O}{\hat{i}_L} \cdot \frac{\hat{i}_L}{\hat{v}_C} = \frac{\hat{v}_O}{\hat{d}} \cdot \left(\frac{\hat{i}_L}{\hat{d}}\right)^{-1} \cdot \frac{\hat{i}_L}{\hat{v}_C} = \frac{\hat{v}_O}{\hat{v}_C} \quad (8)$$

where

$$G_{i_L-v_c}(s) = \frac{\hat{i}_L}{\hat{v}_C} = \frac{T_i(s)}{R_i \cdot (1 + T_i(s))} \quad (9)$$

Fig. 7 shows the Bode plots of $G_{v_O-v_C}(s)$.

4.1. PI voltage controller

The PI controller seeks a system response without error in steady state. The integral action reduces the steady state error produced by the proportional controller. The design of this controller is obtained following the structure of Fig. 8.

The expression of the PI controller is given by (10).

$$\mathrm{PI}(s) = 0.20448 \cdot \frac{s + 4270}{s} \quad (10)$$

Fig. 9 shows the Bode plots of the voltage loop with the controller exposed in Fig. 8 and it is defined as $T_V(s) = G_{v_O-v_C}(s) \cdot \beta \cdot \mathrm{PI}(s)$. The voltage loop with the PI controller has the following stability characteristics: f_{CV} = 780 Hz (gain crossover frequency), PM = 96.7°, GM = 6 dB.

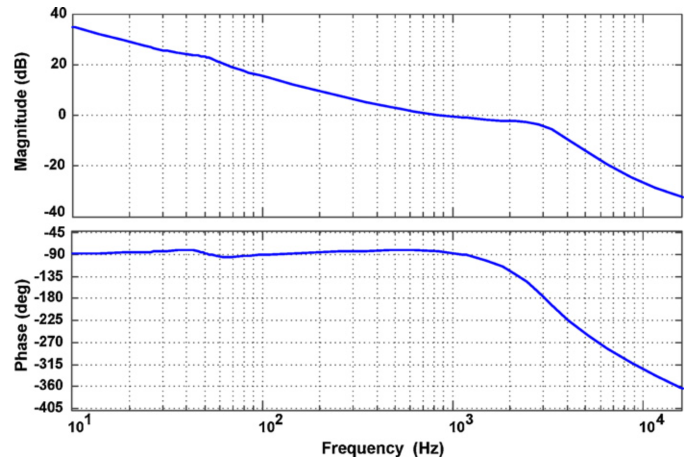


Fig. 9. Bode plots of the voltage loop with a PI controller.

4.2. Two-degree of freedom voltage controller (2DOF)

The 2DOF control technique allows dealing with the system perturbations and reference variations. This technique processes independently the reference signal and output and it presents different tuning methods. The implementation of this technique provides greater robustness than the one degree of freedom techniques [16–18].

The following transfer functions are obtained from Fig. 10:

$$G_{v_O\text{-}v_{ref}}(s) = \frac{\hat{v}_O}{\hat{v}_{ref}} = \frac{G_{v_O\text{-}v_C}(s) \cdot C_1}{1 + (C_1 + C_2) \cdot G_{v_O\text{-}v_C}(s) \cdot \beta} \quad (11)$$

$$G_{v_O\text{-}p}(s) = \frac{\hat{v}_O}{\hat{p}} = \frac{1}{1 + (C_1 + C_2) \cdot G_{v_O\text{-}v_C}(s) \cdot \beta} \quad (12)$$

The controller design must satisfy the following conditions:

$$G_{v_O\text{-}v_{ref}}(s) = \frac{\hat{v}_O}{\hat{v}_{ref}} \approx \frac{1}{\beta} \quad (13)$$

$$G_{v_O\text{-}p}(s) = \frac{\hat{v}_O}{\hat{p}} \to 0 \quad (14)$$

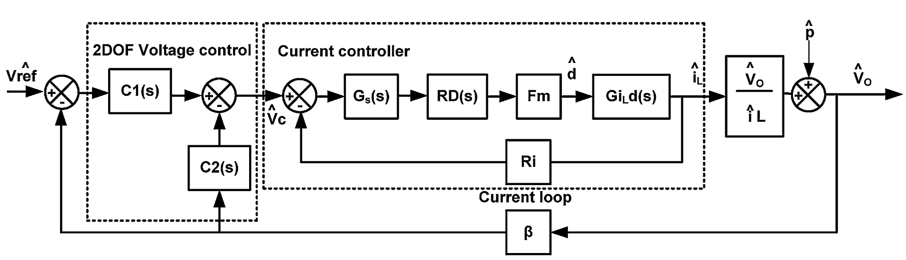


Fig. 10. ACC with 2DOF controller.

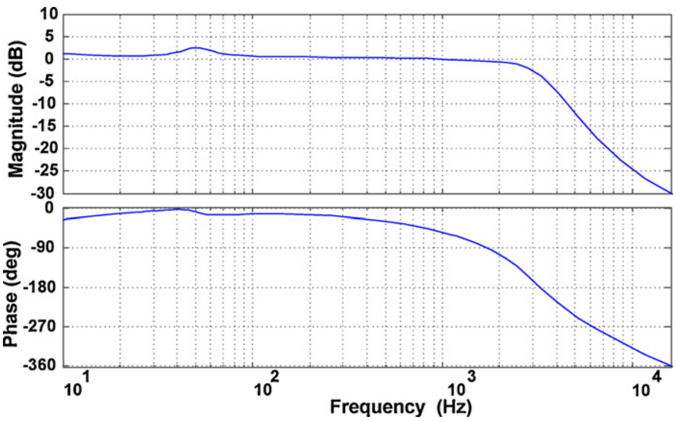


Fig. 11. Bode plots of the voltage loop with 2DOF controller.

The controllers, both C_1 and C_2, are designed according to (14) and (13) and these are presented in (17) and (18).

$$C_2 = 0.0006344 \cdot \frac{s + 1.14e4}{s} \tag{15}$$

$$C_1 = 0.26 \tag{16}$$

The voltage loop gain is defined as:

$$T_V(s) = (C_1 + C_2) \cdot G_{v_O_v_C}(s) \cdot \beta \tag{17}$$

The voltage loop gain with 2DOF controller exhibits the following stability characteristics: f_{Cv} = 797 Hz, PM = 88.85°, GM = 6.3 dB.

Fig. 11 shows the Bode plots of the voltage loop with 2DOF controller.

4.3. Resonant voltage controller

In this section a P + resonant voltage controller was designed as shown in Fig. 12. This controller aims to improve the reference tracking and the attenuation of multiple of fundamental spectral components.

$$G_{V_{res}}(s) = P + Res_C = C + \sum_{h=1}^{7} \frac{K_h \cdot B_h \cdot s}{s^2 + B_h \cdot s + \omega_h^2}, h = odd \tag{18}$$

where P is the controller proportional gain designed to perform with the adequate gain and phase margins, in this case P = 0.26. The other parameters of (18) were explained in Section 3.

The controller parameters values are presented in Table 2:

In Fig. 13 the Bode plots was obtained through the expression $T_V(s) = G_{V_{res}}(s) \cdot G_{v_O_v_C}(s) \cdot \beta$

The voltage loop with the P + resonant controller has the following stability characteristics f_{Cv} = 910 Hz, PM = 115°, GM = 7.2 dB.

It is possible to see in Fig. 13 that the phase is 0 at harmonic frequencies; this means that the controller has a resistive behavior. The decreasing value at high frequencies allows a reduction in the harmonic voltage and a THD_v reduction.

Table 2
Resonant controller parameters.

Harmonic	Gains		BW	
1	K_1	28	B_1	2·π·0.5
3	K_3	12	B_3	2·π·1.5
5	K_5	8	B_5	2·π·2.5
7	K_7	6	B_7	2·π·3.5
9	K_9	4	B_9	2·π·4.5
11	K_{11}	2	B_{11}	2·π·5.5

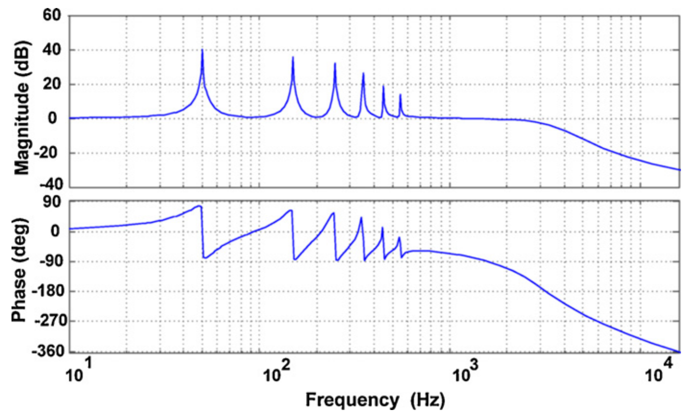


Fig. 13. Bode plots of voltage loop with P + resonant controller.

4.4. Repetitive controller

Repetitive control theory is based on the Internal Model Principle (IMP) and it is capable of tracking periodic references and rejecting periodic disturbances [19].

The concept of IMP is interpreted in the frequency domain as the introduction of high gain in the frequency components related to the signals to be followed or rejected [20]. The repetitive loop has an infinite gain at all frequencies that are multiples of $1/T$, where T is the fundamental period of the reference signal. This feature ensures disturbance rejection and zero error tracking the reference signal.

Basically, the repetitive controller is composed by a delay e^{-sT} and a positive feedback that introduces a high gain at harmonic frequencies [21,22]. The introduction of a low pass filter is convenient, which can be IIR or FIR [23–26], in order to attenuate the gain at those frequencies. The system behavior is less certain at these frequencies than at harmonics of the fundamental signal. Fig. 14 shows the repetitive controller block diagram implemented, where K_r is the repetitive control gain (K_r = 0.4) and $Q(s)$ is a infinite impulse response (IIR) low pass filter of second order.

$$Q(s) = \frac{1}{(s^2/\omega_q^2) + (2\varepsilon s/\omega_q) + 1} \tag{19}$$

where ε is the damping factor (ε = 0.707) and ω_q is the filter cutoff frequency expressed in rad/s (ω_q = 2·π·400).

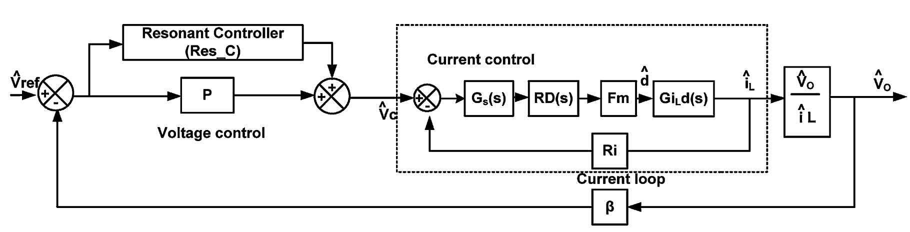


Fig. 12. ACC with P + resonant controller.

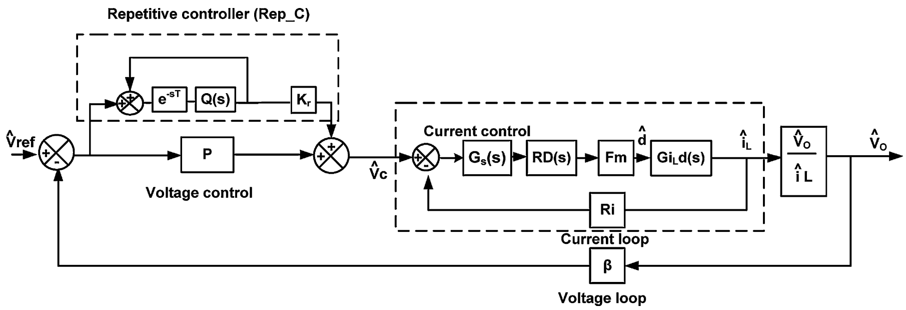


Fig. 14. ACC with P + repetitive controller.

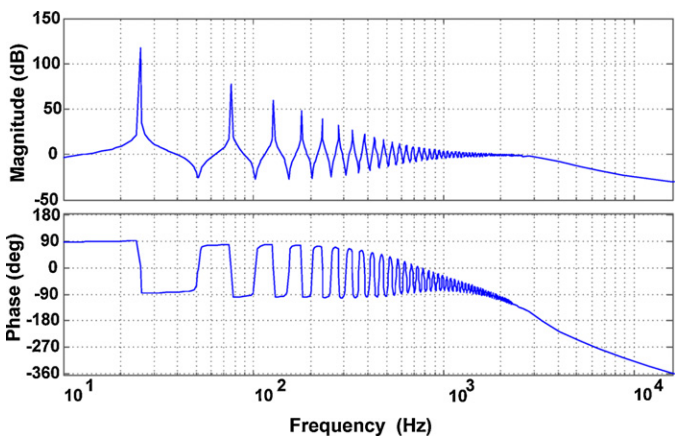


Fig. 15. Voltage loop Bode diagram using P + repetitive controller.

P is calculated in the same way that was calculated for the PI proportional gain.

Fig. 15 shows the bode diagram for the voltage loop presented in Fig. 14, it is defined by:

$$T_{V_{Rep_C}}(s) = (P + Rep_C) \cdot G_{v_O_v_C}(s) \cdot \beta \tag{20}$$

where $G_{v_O_v_C}(s)$ is the transfer function, which relates control voltage to output voltage.

In Fig. 15, the voltage loop with the P + resonant controller has the following stability characteristics f_{Cv} = 569 Hz, PM = 81.5°, GM = 6.1 dB.

The output impedance has a resistive behavior at harmonic frequencies of fundamental. This behavior is ideal to minimize the THD_V and it is similar to repetitive controller behavior.

From Figs. 13 and 15, it is possible to see that through resonant controllers the frequency to delete can be chosen, while through repetitive controller implementation, the action is performed automatically for frequency multiples of the fundamental. Additionally, the implemented repetitive controller has a lower bandwidth than the resonant controller in the voltage loop.

5. Simulation results

The simulation results in island mode are shown below. The system has been simulated in PSIM 7.05 [27].

Figs. 16–19 show the output voltage and current waveforms for a nonlinear load using PI, 2DOF, resonant and repetitive controllers, explained in the previous section. The nonlinear load corresponds to a full wave rectifier with capacitive output filter 1.5 mF and a resistance of 85 Ω. The rectifier has no input inductance so that the results presented are a highly nonlinear load with crest factor of 4.6 when it is connected to an ideal sinusoidal voltage 230 V_{RMS} grid. The output power in this case is 1200 VA approximately. All simulations were performed in islanded situation.

Table 3 summarizes the inverter output voltage THD_V using the four controllers feeding linear and nonlinear loads. It is possible to see that the PI controller has the worst response in terms of THD_V reduction: this response is produced with nonlinear loads. Including a 2DOF control, THD_V is reduced 45% compared with the use of PI controller. Moreover, the implementation of the repetitive controller and the resonant controller gives the best results. This is mainly due to the use of a resonant controller which permits to

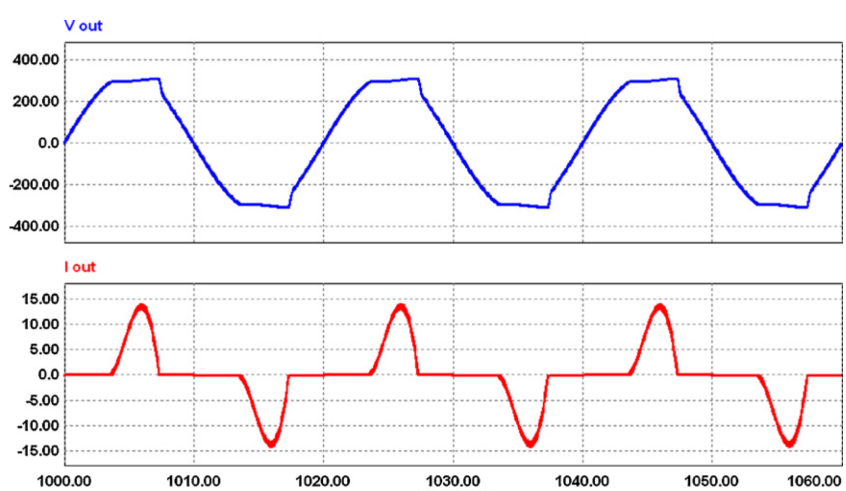


Fig. 16. Inverter output waveforms with a PI controller (output voltage and output current).

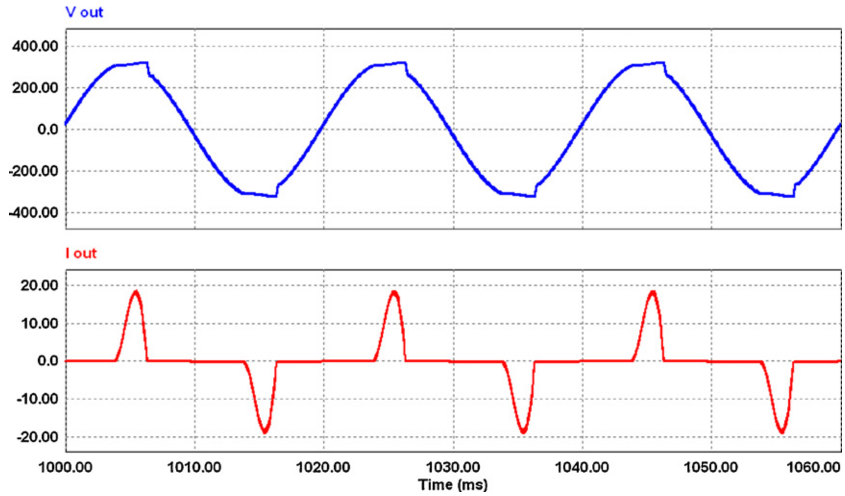


Fig. 17. Inverter output waveforms with a 2DOF control (output voltage and output current).

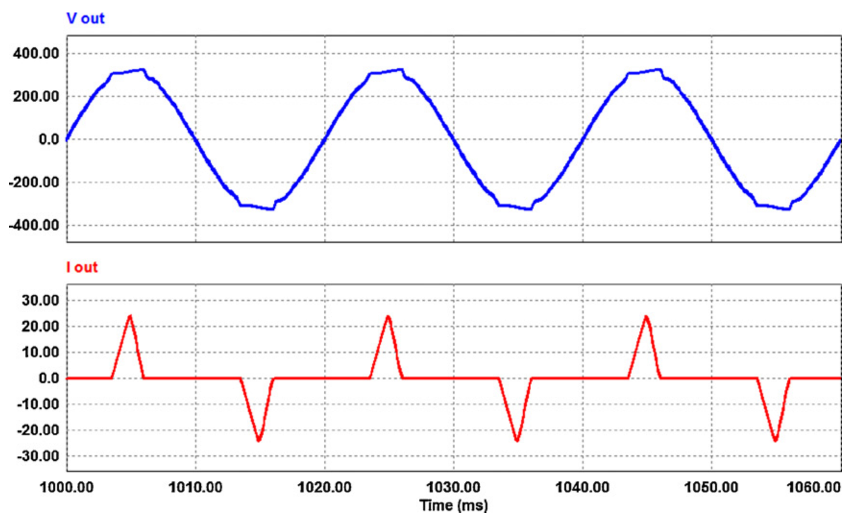


Fig. 18. Inverter output waveforms with a *P* + resonant controller (output voltage and output current).

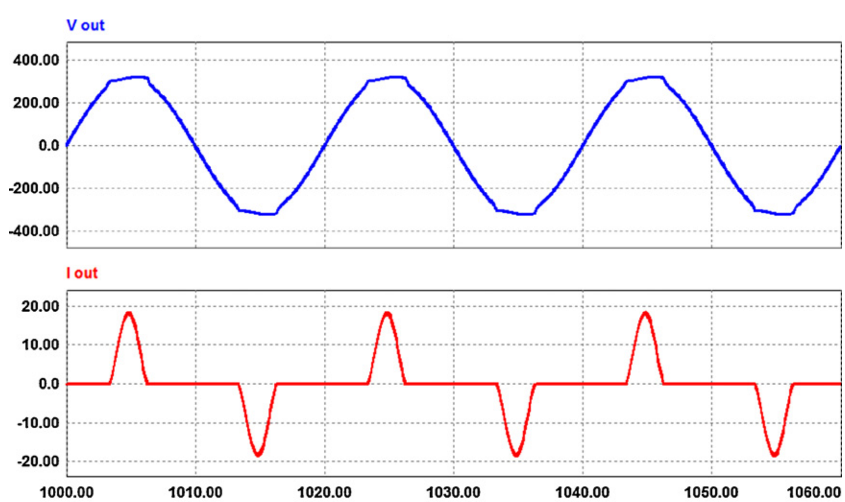


Fig. 19. Inverter output waveforms with a *P* + repetitive controller (output voltage and output current).

Table 3
THD_v results.

Controller	Load	THD_v (%)
PI	Linear	0.87
	Nonlinear	7.6
2DOF	Linear	0.9
	Nonlinear	4.2
Resonant	Linear	0.86
	Nonlinear	2.92
Repetitive	Linear	0.89
	Nonlinear	2.8

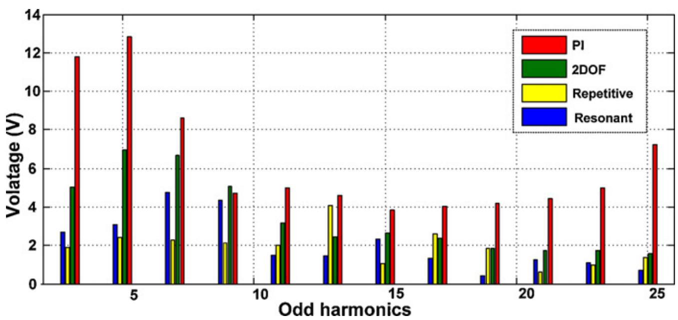


Fig. 20. Harmonics of the inverter output voltage supplying a nonlinear load.

select the harmonic that has to be removed as well as its gain. The repetitive controller has a similar behavior but in this case the gain is set automatically according to the characteristics of the controller design.

Fig. 20 shows the comparative harmonic contents of the inverter output voltage supplying the previously defined nonlinear load with different controllers.

6. Conclusions

In this paper it was presented the design, implementation and simulation results of four types of controllers in the voltage loop for an inverter operating isolated with the aim to analyze the reduction of THD_v with a nonlinear load (a full-wave rectifier with a crest factor of 4.6). In all cases, except for the controller PI, the THD_v levels were lower than 5%: this value is recommended by the standard IEEE 519. Finally, the controllers, that showed the best behavior from the point of view of THD_v reduction (lower that 3%), were resonant controller and repetitive controller. It is worth pointing out that repetitive controllers have the advantage of easy implementation and low computational load, which implies programming a delay and a filter, while for a resonant controller it is necessary to set a resonator for each harmonic that has to be eliminated.

Acknowledgements

This work was supported by the Spanish Ministry of Science and Innovation under Grant ENE2009-13998-C02-02. The first author thanks the support of the Instituto Politécnico Nacional (IPN), the Comisión de Operación y Fomento de Actividades Académicas (COFAA), the Secretaria de Educación Pública and the Agencia Española de Cooperación Internacional para el Desarrollo (AECID).

References

[1] Poullikkas A. Implementation of distributed generation technologies in isolated power systems. Renewable and Sustainable Energy Reviews 2007;11(January (1)):30–56.
[2] Lidula NWA, Rajapakse AD. Microgrids research: a review of experimental microgrids and test systems. Renewable and Sustainable Energy Reviews 2011;15(January (1)):186–202.
[3] Panwar NL, Kaushik SC, Kothari S. Role of renewable energy sources in environmental protection. Renewable and Sustainable Energy Reviews 2011;15(April (3)):1513–24.
[4] Velasco D, Trujillo CL, Peña RA. Power transmission in direct current. Future expectations for Colombia. Renewable and Sustainable Energy Reviews 2011;15(January (1)):759–65.
[5] Eltawil MA, Zhengming Z. Grid-connected photovoltaic power systems: technical and potential problems. Renewable and Sustainable Energy Reviews 2010;14(January (1)):112–29.
[6] Khan N, Abas N. Comparative study of energy saving light sources. Renewable and Sustainable Energy Reviews 2011;15(January (1)):296–309.
[7] Kuo BC, Golnaraghi F. Automatic control systems. John Wiley & Sons; 2002.
[8] Araki M, Taguchi H. Tutorial paper. Two-degree-of-freedom PID controllers. International Journal of Control Automation and Systems 2003;1(December (4)).
[9] Sato Y, Ishizuka T, Nezu K, Kataoka T. A new control strategy for voltage-type PWM rectifiers to realize zero steady-state control error in input current. IEEE Transactions on Industry Applications 1998;34(May/June (3)):480–6.
[10] Tzou Y, Jung S, Yeh H. Adaptive repetitive control of PWM inverters for very low THD AC voltage regulation with unknown loads. IEEE Transactions on Power Electronics 1999;14(September (5)):973–98.
[11] Mohan N, Underland TM, Robbins WP. Power electronics: converters, applications, and design. 3rd ed. John Wiley & Sons; 2003.
[12] Erickson RW. Fundamental of power electronics. Norwell, MA: Kluwer; 1997.
[13] Jung YS, Lee JY, Youn MJ. A new small signal modeling of average current mode control. In: Power electronics specialists conference, 1998, PESC 98 Record. 29th annual IEEE, vol. 2. 1998. p. 1118–24.
[14] Sable DM, Ridley RB. Comparison of performance of single loop and current injection control for PWM converters that operate in both continuous and discontinuous modes of operation. IEEE Transactions on Power Electronics 1992;7(January (1)):136–42.
[15] Zmood DN, Holmes DG. Stationary frame current regulation of PWM inverters with zero steady state error. IEEE Transactions on Power Electronics 2003;18(May (3)):814–22.
[16] Rovira AA, Murrill PW, Smith CL. Tuning controllers for setpoint changes. Instruments and Control Systems 1969;December:67–9.
[17] Araki M. PID control systems with reference feed forward (PID-FF control systems). In: Proc. of 23rd SICE annual conference. 1984. p. 31–2.
[18] Araki M. Two-degree-of freedom control system. Part I. Systems and Control 1985:649–56.
[19] Francis BA, Wonham WM. The internal model principle of control theory. Automatica 1976;12(September (5)):457–65.
[20] Hara S, Yamamoto Y, Omata T, Nakano M. Repetitive control system: a new type servo system for periodic exogenous signals. IEEE Transactions on Automatic Control 1988;33(July (7)):659–68.
[21] Broberg HL, Molyet RG. Reduction of repetitive errors in tracking of periodic signals: theory and application of repetitive control. In: First IEEE conference on control applications, vol. 2. 1992. p. 1116–21.
[22] Chen S, Lai YM, Tan S, Tse CK. Analysis and design of repetitive controller for harmonic elimination in PWM voltage source inverter systems. IEEE Transactions on Power Electronics 2008;1(4):497–506.
[23] Chen B, Zha X, Gong J, Guo S, Sun J. Realization and improvement of repetitive control in rotating frame for active power filter system. In: Applied power electronics conference and exposition (APEC) 2010. Twenty-fifth annual IEEE. 2010. p. 887–94.
[24] Chen S, Lai YM, Tan SC, Tse CK. Optimal design of repetitive controller for harmonic elimination in PWM voltage source inverters. In: Telecommunications energy conference, 2007. INTELEC 2007, 29th international. 2007. p. 236–41.
[25] Zhou K, Wang D. Unified robust zero-error tracking control of CVCF PWM converters. IEEE Transactions on Circuits and Systems: Fundamental Theory and Applications 2002;49(April (4)):492–501.
[26] Chen M, Yao W, Li M, Qian Z, Yuan X. Design and analysis of high performance control strategy for UPS with repetitive control. In: Telecommunications energy conference, 2006. INTELEC '06, 28th annual international. 2006. p. 1–4.
[27] PSIM 7.0. Users guide. Powersim Inc.; 2006.